© 2016. Published by The Company of Biologists Ltd | Journal of Experimental Biology (2016) 219, 2823-2827 doi:10.1242/jeb.143388

Smart Mechanical Dipole: a device for the measurement of sphere motion in behavioral and neurophysiological experiments

Hendrik Herzog*, Joachim Mogdans and Horst Bleckmann

ABSTRACT

Fluid motion and pressure fields induced by vibrating spheres are frequently used to investigate the function of biological mechanosensory systems and artificial sensors. The calibration of the sphere motion amplitude (displacement, velocity, acceleration), time course and vibration direction often demands expensive equipment. To mitigate this requirement, we have developed a high-quality, low-cost device that we term a 'Smart Mechanical Dipole'. It provides real-time measurement of sphere acceleration along three axes and can be used to obtain an accurate stimulation trace. We applied digital filtering to equalize the frequency response of the vibrating sphere, which also reduced unwanted amplitude and frequency changes in the hydrodynamic signal. In addition, we show that the angular orientation of the rod to which the sphere was attached, i.e. axial versus transverse, but not the immersion depth of the sphere affected sphere vibration behavior.

KEY WORDS: Flow field, Lateral line, Hydrodynamic stimulation, Miniature accelerometer, Vibrating sphere, Digital signal processor

INTRODUCTION

The lateral line system of fishes is highly sensitive to water movements and pressure gradients (e.g. Coombs et al., 2014). A vibrating sphere generates a well-defined pressure and flow field (Kalmijn, 1988) and has therefore frequently been used to investigate lateral line function (e.g. Harris and van Bergeijk, 1962; Engelmann et al., 2002; Coombs and Patton, 2009). Typically, the sphere is attached to a small rod driven by a mini-shaker (an electro-dynamic or piezoelectric device that generates small vibrations). Unfortunately, equal input voltages fed into the mini-shaker may lead to different sphere vibration amplitudes across stimulus frequencies (e.g. Bleckmann et al., 1991). As a consequence, vibrating sphere amplitudes are measured across frequencies prior to the experiments; for example, with hydrophones (Coombs et al., 1996), laser interferometers (Asadnia et al., 2015), distance transducers (Künzel et al., 2011) or large vibration sensors placed inside the rod (McConney et al., 2009) or a vibrating sphere (diameter 57 mm; Gaspard et al., 2013) to calibrate sphere movement. To compensate for unwanted amplitude variations, the input voltages are adjusted manually to achieve a flat frequency response in most cases. Bohnenberger et al. (1983) used an active vibration control implemented into the mini shaker (see also Fuller et al., 1996). In addition to unwanted amplitude variations, resonant effects may alter the time course of the signals. Moreover, the sphere often not only moves in the shaker axis but – depending on the frequency – also may move in other directions (H.B., personal observations). This has not been considered in any previous study. Lateral line receptors (neuromasts) are sensitive to stimulus amplitude (Görner, 1963) and direction (Flock, 1965). Thus, unwanted and uncontrolled sphere movements may alter peripheral and central responses of the lateral line. The same argument applies to other hydrodynamic receptor systems (e.g. Bleckmann, 1994). To control for unwanted sphere movements, a monitoring of sphere motion in three dimensions is required. Here, we present a low-cost measuring device termed a 'Smart Mechanical Dipole' (SMD) based on miniature accelerometers mounted inside a small (diameter 14 mm) vibrating sphere. The SMD monitors sphere motion in three dimensions in real-time and can therefore be used for fast and continuous calibration and adjustment of sphere motion during stimulation in behavioral and neurophysiological experiments.

MATERIALS AND METHODS

A vibrating sphere (diameter 14 mm), consisting of two halves, was connected to a carbon tube (Fig. 1). The sphere was equipped with an electronic board containing a miniature accelerometer (model ADXL330, 4×4×1.5 mm^3, Analog Devices Inc., Norwood, MA, USA) that allowed us to monitor the sphere movement in three dimensions (metering range ±29.4 m s^{-2}). The electronic circuit of the SMD (Fig. 1A) was assembled according to the data sheet provided by the manufacturer (online data sheet: http://www.analog.com/static/imported-files/data_sheets/ADXL330.pdf) and mounted on a round piece (diameter 8 mm) of universal printed circuit board (PCB) with soldering pads spaced 1.27 mm apart. The accelerometer was glued bottom-up to the center of the PCB. To reduce electronic noise, each accelerometer output was bypassed by a capacitor of 10 nF limiting the frequency bandwidth to about 500 Hz. The supply voltage was buffered by a 100 nF capacitor connected to the ground. The four capacitors were soldered to the pads of the PCB. Insulated copper wires (diameter 0.15 mm) were used for all connections on the PCB. Acceleration outputs, supply voltage, and common and self-test input were connected to an additional supply PCB mounted outside the water. The PCBs were connected by insulated copper wires running inside the carbon tube and soldered to flexible unshielded cables (0.14 mm^2, AWG 26) after leaving the carbon tube. The supply PCB carried two alkaline batteries (type LR03) providing 3 V power to the accelerometer, three BNC plugs for the accelerometer outputs and two switches for power on/off and self-test of the circuit. The output voltage of the accelerometer is a function of acceleration and supply voltage. Therefore, constant supply voltage (<3.6 V) is needed. This requires either a precision voltage regulator or a frequent battery check. A cavity (diameter 8 mm, depth 3 mm) was drilled into each half of the sphere to mount the PCB carrying the accelerometer (Fig. 1B). The assembled PCB inside the sphere was sealed with polyurethane lacquer. After drying of the sealant, 2-component epoxy resin was

Institute of Zoology, University of Bonn, Poppelsdorfer Schloss, Bonn D-53115, Germany.

*Author for correspondence (hendrik.herzog@uni-bonn.de)

H.H., 0000-0003-0693-3007

Received 17 May 2016; Accepted 10 July 2016

Journal of Experimental Biology (2016) 219, 2823-2827 doi:10.1242/jeb.143388

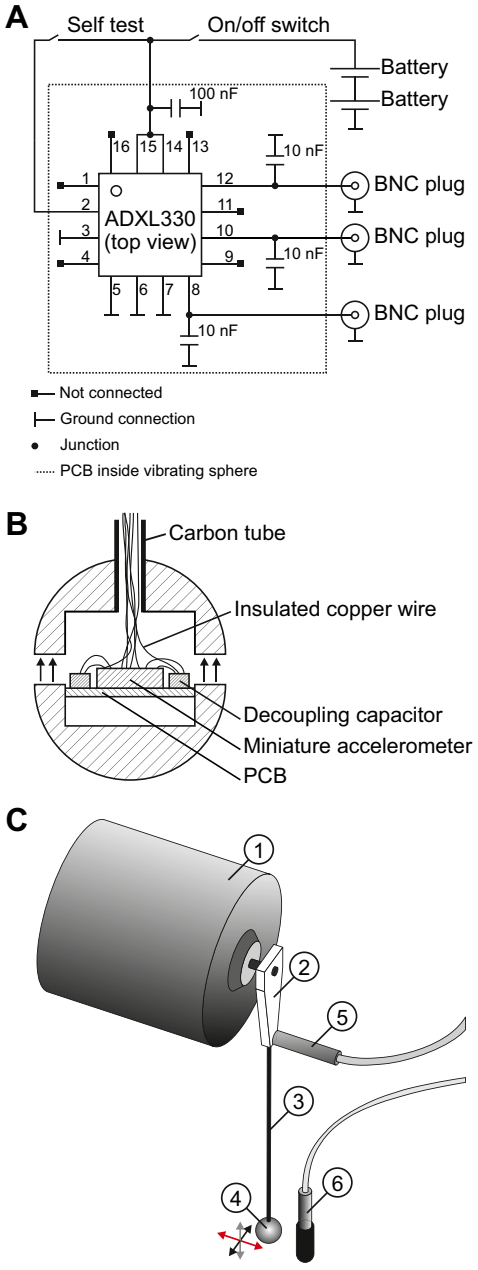

Fig. 1. The Smart Mechanical Dipole (SMD). (A) Electronic circuitry based on the miniature accelerometer (ADXL330) mounted on a printed circuit board (PCB). Numbers 1 to 16 refer to soldering pads of the miniature accelerometer. (B) Assembly of the half-sectioned sphere, isolated copper wires running inside a carbon tube and the PCB featuring the accelerometer. (C) Experimental setup showing the mini-shaker (1), acrylic holder (2), vertically oriented carbon tube (3), vibrating sphere (4), displacement transducer (5) and hydrophone (6). Arrows give the orientation of the accelerometer axes (red: in shaker axis, black: transverse, gray: vertical).

used to connect the two half spheres and to attach the carbon tube (length 120 mm, outer diameter 2 mm, inner diameter 1 mm) to the upper half of the sphere. Finally, the carbon tube was fixed to an acrylic holder that was bolted to a mini-shaker (model VT-20, Sigmatest, Gottmadingen, Germany) powered by an amplifier (PA25E, Ling Dynamic Systems, Royston, UK).

The mini-shaker driving the SMD was mounted on a guide rail system (isel Germany AG, Eichenzell, Germany) that allowed us to lower the sphere into the water basin (diameter 80 cm, water level 15 cm, sphere was submerged 30 mm for experiment 1, see below). The mini-shaker was mounted horizontally, i.e. it produced horizontal to and fro movements of its bolt.

In experiment 1, the acrylic holder with the attached carbon rod and sphere were mounted vertically and at a right angle to the mini-shaker (Fig. 1C; e.g. Künzel et al., 2011). Thus, movements of the mini-shaker caused movements of the holder, rod and sphere predominantly in the shaker axis (but see Results). A frequency sweep from 10 to 100 Hz (constant amplitude, duration 60 s) and constant-frequency trains of 10, 20, 30, 40, 50, 60, 70, 80, 90 and 100 Hz with identical voltage amplitudes and a duration of 500 ms each were generated with the software Spike2 (Cambridge Electronic Design, Cambridge, UK) and a D/A converted (Power 1401, Cambridge Electronic Design). To compensate for possible frequency-dependent amplitude variations, the D/A output signal was fed into a digital signal processor (MiniDSP, Monacor International, Bremen, Germany) that was connected to the power amplifier (for alternative compensation procedures, see Miyoshi and Kaneda, 1988; Nelson et al., 1992; Corteel et al., 2002). To measure the uncompensated response of the vibrating sphere, signal compensation was deactivated (2-channel crossover software: 2way Advanced, miniDSP Ltd, Hong Kong, China; https://www.minidsp.com/products/plugins/2way-advanced-detail).

In addition to the three outputs of the SMD, we recorded the voltage output of the D/A converter and the digital signal processor (DSP), measured the displacement of the acrylic holder (above the water level) using a capacitive displacement transducer (4810, LOT-Oriel, Darmstadt, Germany), and the pressure generated by the sphere using a hydrophone (model 8103, Brühl & Kjær) connected to a charge amplifier (model 2635, Brühl & Kjær). The hydrophone was placed at a distance of 10 mm (surface to surface) from the sphere (Fig. 1C). Signals were A/D converted (Power 1401, Cambridge Electronic Design) and stored on a PC using the software Spike2 (Cambridge Electronic Design). All signals except the hydrophone trace were 0.1 Hz high-pass filtered. Because of low-frequency baseline drifts, the hydrophone signals were high-pass filtered with a corner frequency of 2 Hz. In the case of the constant amplitude sweep, root mean square (rms) values were calculated over a time window of 0.5 s for each recording trace to plot and to compare the amplitudes of the recorded signals.

In neurophysiological experiments, it may be necessary to alter the angle of the rod holding the sphere by 10 or 20 deg to avoid contact with other parts of the experimental set-up, like the fish or electrode holder (Mogdans and Kröther, 2001; Engelmann et al., 2002). In other experiments, the rod holding the sphere was not mounted orthogonally but axially, i.e. in the shaker axis (e.g. Coombs and Janssen, 1990; Coombs, 1994). Therefore, we also investigated how the mounting of the rod influences sphere vibration.

In experiment 2, the rod was oriented either in the axial (parallel to shaker motion) or in the orthogonal (perpendicular to shaker motion) direction (Figs S1 and S2). To achieve this, a small plastic adapter with two orthogonal screws was positioned between the shaker axis and the acrylic holder. In each case, the angular orientation (0, 10, 20 deg) and the water depth (10, 15, 20, 25 mm) were varied and frequency sweeps (see above, 10 repetitions) were presented. rms values of the acceleration along the three axes were used to investigate the influence of mounting and submersion depths on sphere vibration behavior.

RESULTS AND DISCUSSION

Experiment 1 revealed that the acceleration, pressure and displacement rms amplitudes and their phase relationships

Journal of Experimental Biology (2016) 219, 2823-2827 doi:10.1242/jeb.143388

depended on stimulus frequency (Fig. 2). When the non-equalized sweep (10 to 100 Hz) was driving the sphere, large changes in acceleration amplitude were observed in the shaker axis and in the transverse direction of sphere motion (Fig. 2A, red lines).

The acceleration in the shaker axis increased with rising frequency, resulting in a large peak at 30 Hz, and decreased again with further increasing frequency. This indicates resonant effects caused by the spring-load properties of the sphere and the mounting rod used in our particular setup. The transverse acceleration exhibited a maximum at 33 Hz and a side-peak at 30 Hz. This implies that the sphere was moving not only in the axial but also in the transverse direction. Only minor changes in acceleration (at 30, 67 and 74 Hz) were observed in the vertical direction of sphere motion (Fig. 2A, Vertical acceleration trace, red line). The pressure signal was in agreement with the acceleration signal in the shaker axis (Fig. 2A). This is expected from physics as compression of the water is induced by the acceleration of the sphere (Kalmijn, 1988). The rms displacement of the sphere holder peaked at 29 Hz, exhibited a trough at 32 Hz, peaked again at 45 Hz and then decreased again above 45 Hz (Fig. 2A). Fig. 2 indicates that the displacement amplitudes measured with the capacitive sensor above the water level did not reflect the motions of the submerged sphere. This most likely was due to water-induced friction.

To compensate for frequency-dependent amplitude changes, a transfer function (three notch filters, two high-shelf filters, one low-shelf filter, 20 iterations) was applied by the DSP (Fig. 2A, DSP output trace, black line). This resulted in a linearization of the frequency response of the vibrating sphere in the shaker axis. However, some frequency-dependent amplitude modulations were still present in both the in shaker axis signal and the pressure signal. In addition, displacement amplitudes increased strongly in the low-frequency range (10–25 Hz), which may induce limitations in dynamic amplitude range due to the maximum displacement range of the mini-shaker. The removal of the 30 Hz peak in the in shaker axis signal also reduced the smaller peaks in the acceleration signals in the transverse and vertical axis (Fig. 2A, Vertical acceleration and Transverse acceleration traces). However, the increase in signal amplitude for frequencies above 40 Hz increased the vibration amplitude in the vertical axis, resulting in a peak at 74 Hz. The equalization of the signals delivered to the shaker resulted in a greater linearity of the sphere motion along the main axis of vibration. Nonetheless, transverse sphere motions could not be completely avoided.

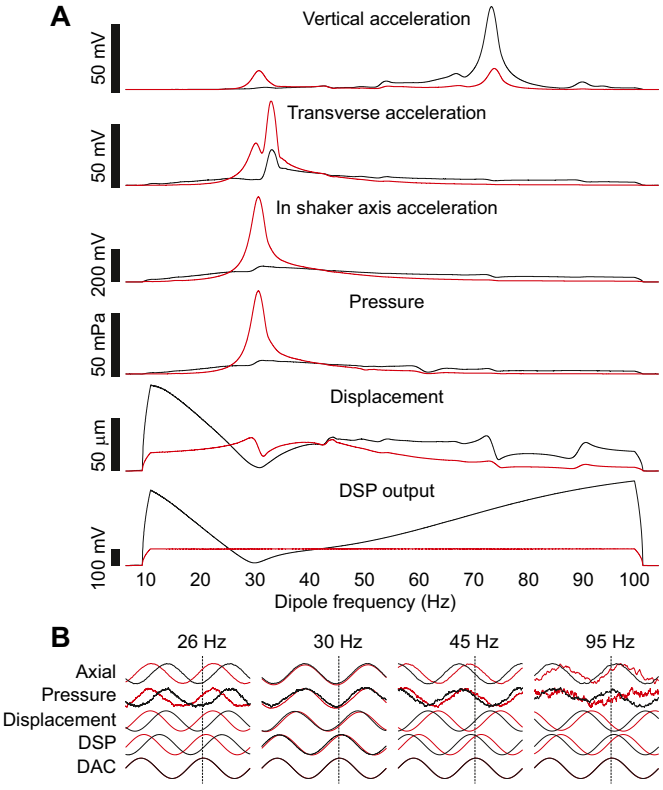

Fig. 2. Frequency-dependent oscillation amplitude and orientation of the SMD. (A) Frequency sweep from 10 to 100 Hz. From bottom to top: root mean square (rms) output signal of the digital signal processor (DSP), rms displacement of the acrylic holder, rms pressure signal and rms acceleration in the shaker axis, traverse axis and vertical axis (along the carbon tube). Curves are averaged over nine runs (standard deviations were smaller than line width and are not shown). (B) Magnified waveforms for the frequencies 26, 30, 45 and 95 Hz. From bottom to top: output signals of the D/A converter (DAC) and the DSP, displacement, pressure and acceleration in the shaker axis (axial). All traces are normalized to the maximal amplitudes within the time period of two wave cycles. Red lines in A and B: responses of the vibrating sphere to the non-equalized DSP output. Black lines in A and B: results of the frequency equalization by means of the digital signal processor. Note the phase shift between the DAC and the DSP traces following equalization.

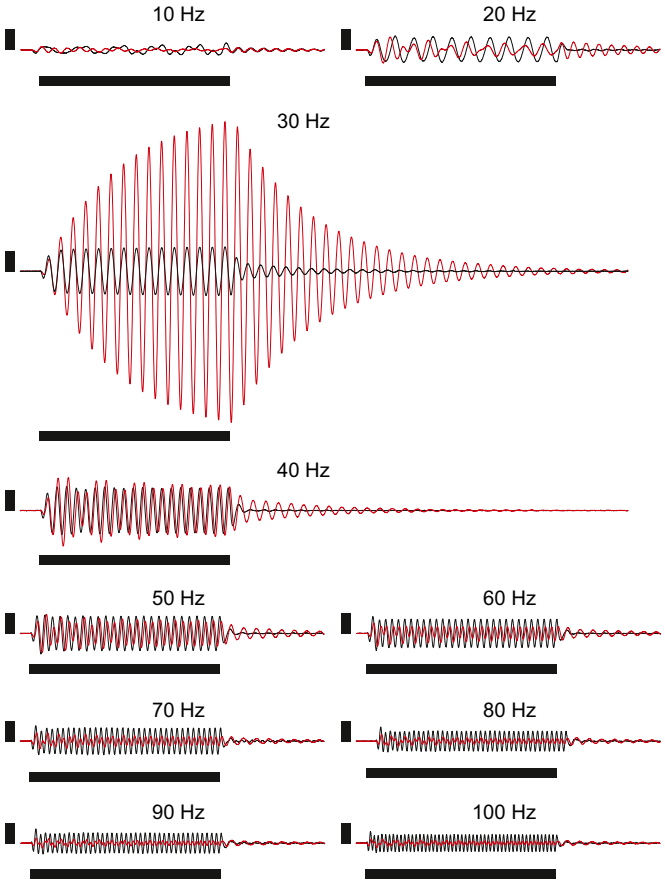

Fig. 3. Transient behavior of the SMD. Short wave trains of constant frequency and duration were applied. Red lines: responses of the vibrating sphere to the non-equalized DSP output. Black lines: responses of the vibrating sphere after frequency equalization by means of the DSP. Output signals of the SMD in the shaker axis are shown (vertical bars indicate 100 mV). Horizontal bars indicate duration (500 ms) of the signal of the D/A converter. Lines show mean values of 10 signals each. Note the beating effects at stimulus onset, the post-pulse oscillations and deviations in vibration amplitude at different stimulus frequencies.

Journal of Experimental Biology (2016) 219, 2823-2827 doi:10.1242/jeb.143388

Comparing the non-equalized signals at distinct points in time showed that, for frequencies <30 Hz, the output signal of the DSP was almost in phase with the displacement and acceleration measured in the shaker axis (Fig. 2B, red lines). For frequencies between 30 and 40 Hz, slight phase shifts occurred between the acceleration in the shaker axis, the pressure signal and the DSP output signal. For frequencies >40 Hz, acceleration in the shaker axis, pressure, displacement and the DSP output signal were phase shifted. If signal filtering was applied, the phase between the electrical signals of the DSP output and the D/A converter output was additionally shifted (Fig. 2B, DSP and DAC traces). This effect was due to the properties of the IIR filters used by our DSP setup and might be avoided by using FIR filters instead (see theoretical details in Oppenheim et al., 1989, for example). A substantial phase shift between the electrical signal driving the sphere and the mechanical signals was apparent in each case; thus, only the acceleration signals or the hydrophone trace revealed the actual phase of sphere motion.

Verification of sphere motion with the constant-frequency pulses revealed that at frequencies between 20 and 40 Hz, the acceleration signals in the shaker axis increased in amplitude and lasted substantially longer than the electrical signal that was driving the sphere (Fig. 3, red lines), i.e. the frequency range where the largest vibration amplitudes were present in the non-equalized frequency sweep verification (Fig. 2, black lines). In particular, in case of the 30 Hz pulse, the acceleration signal was strongly amplitude modulated and lasted about three times longer than the electrical signal (see Fig. 3). However, amplitude modulations and beating effects were also apparent at other stimulus frequencies (Fig. 3). If the same filter settings were applied to the DSP that were used to equalize the response of the sphere to a linear sweep (Fig. 2A), the frequency-dependent amplitude compensation substantially altered the amplitude and the time course of the vibrating sphere: amplitudes were more similar across frequencies, amplitude modulations were reduced, vibrations lasted a shorter time and the beating effects within the initial portion of the pulses were less apparent. These effects demonstrate the benefit of compensation of the frequency response for the amplitude and time course of the vibration signals.

Experiment 2 revealed that orthogonal mounting of the carbon rod relative to the shaker axis reduced linearity of sphere motion along the main axis of vibration (compare Figs S1 and S2). However, transverse sphere motions occurred even in the case of axial mounting (Fig. S2). In contrast, small angular deviations in rod orientation and moderate variation of the water level only slightly influenced the measured acceleration signals.

In summary, our data show that the SMD provides information about the three-dimensional movement of the vibrating sphere. In terms of frequency-dependent signal amplitudes and phase, the time course of the axial acceleration output of the SMD was similar to the time course of the pressure measured with a precision hydrophone. The frequency-dependent filtering reduced the amplitude variation, diminished the transverse oscillation and also improved the temporal characteristics of the pulse signal at the resonant frequency. However, the digital filter used in our study was designed for acoustic applications (frequency range 10–20 kHz, amplitude range ±20 dB), which may induce some limitations to very low frequency signals and large amplitude deviations. Moreover, orthogonal sphere mounting, although extensively used in previous experiments, induced larger deviations in the frequency response than axial sphere mounting and should be avoided whenever possible. The SMD is modifiable to the needs of the specific application but, because of the dimensions of the accelerometer (see above), the sphere must have a diameter of at least 8 mm. Moreover, the acceleration signals can be used for optimization of the mechanical setup and for compensation of the frequency response.

Acknowledgements

We thank Vera Schluessel for helpful comments on the manuscript and the micro-mechanic factory staff for assistance with the fabrication of the Smart Mechanical Dipole. In addition, we acknowledge the valuable comments and suggestions of two anonymous reviewers.

Competing interests

The authors declare no competing or financial interests.

Author contributions

The original question, whether the motion in the case of larger spheres is predictable from standard measurement techniques commonly used in our lab, was raised by H.B. The construction, measurements and frequency compensation shown here were performed by H.H. The manuscript was written predominantly by H.H. and J.M. Improvements for analysis and data representation were made by J.M. and H.B.

Funding

The research described in this paper was supported by the Bundesministerium für Bildung und Forschung (BMBF, project number 033 RB 0902A).

Supplementary information

Supplementary information available online at
http://jeb.biologists.org/lookup/doi/10.1242/jeb.143388.supplemental

References

Asadnia, M., Kottapalli, A. G. P., Miao, J., Warkiani, M. E. and Triantafyllou, M. S. (2015). Artificial fish skin of selfpowered micro-electromechanical systems hair cells for sensing hydrodynamic flow phenomena. *J. R. Soc. Interface* **12**, 20150322.

Bleckmann, H. (1994). *Reception of Hydrodynamic Stimuli in Aquatic and Semiaquatic Animals*, Vol. 41 of Progress in Zoology. Stuttgart; Jena; New York: Gustav Fischer Verlag.

Bleckmann, H., Budelmann, B. U. and Bullock, T. H. (1991). Peripheral and central nervous responses evoked by small water movements in a cephalopod. *J. Comp. Physiol. A* **168**, 247-257.

Bohnenberger, J., Seyfarth, E.-A. and Barth, F. G. (1983). A versatile feedback controller for electro-mechanical stimulation devices. *J. Neurosci. Methods* **9**, 335-341.

Coombs, S. (1994). Nearfield detection of dipole sources by the goldfish (*Carassius auratus*) and the mottled sculpin (*cottus bairdi*). *J. Exp. Biol.* **190**, 109-129.

Coombs, S. and Janssen, J. (1990). Behavioral and neurophysiological assessment of lateral line sensitivity in the mottled sculpin, *Cottus bairdi*. *J. Comp. Physiol. A* **167**, 557-567.

Coombs, S. and Patton, P. (2009). Lateral line stimulation patterns and prey orienting behavior in the lake michigan mottled sculpin *Cottus bairdi*. *J. Comp. Physiol. A* **195**, 279-297.

Coombs, S., Hastings, M. and Finneran, J. (1996). Modeling and measuring lateral line excitation patterns to changing dipole source locations. *J. Comp. Physiol. A* **178**, 359-371.

Coombs, S., Bleckmann, H., Fay, R. R. and Popper, A. N. (2014). *The Lateral Line System*. New York: Springer.

Corteel, E., Horbach, U. and Pellegrini, R. (2002). Multichannel inverse filtering of multiexciter distributed mode loudspeakers for wave field synthesis. *Audio Engineering Society Convention 112* (April 2002). http://www.aes.org/e-lib/browse.cfm?elib=11361

Engelmann, J., Hanke, W. and Bleckmann, H. (2002). Lateral line reception in still and running water. *J. Comp. Physiol. A* **188**, 513-526.

Flock, Å. (1965). Electronmicroscopic and electrophysiological studies on the lateral line canal organ. *Acta Otolaryngol.* **199**, 1-90.

Fuller, C. C., Elliott, S. and Nelson, P. A. (1996). *Active Control of Vibration*. London: Academic Press.

Gaspard, J. C., III, Bauer, G. B., Reep, R. L., Dziuk, K., Read, L. and Mann, D. A. (2013). Detection of hydrodynamic stimuli by the Florida manatee (*trichechus manatus latirostris*). *J. Comp. Physiol. A* **199**, 441-450.

Görner, P. (1963). Untersuchungen zur Morphologie und Elektrophysiologie des Seitenlinienorgans vom Krallenfrosch (*Xenopus laevis* Daudin) (in German). *Z. Vergl. Phys.* **47**, 316-338.

Harris, G. G. and van Bergeijk, W. A. (1962). Evidence that the lateral-line organ responds to near-field displacements of sound sources in water. *J. Acoust. Soc. Am.* **34**, 1831-1841.

Kalmijn, A. (1988). Hydrodynamic and acoustic field detection. In *Sensory Biology of Aquatic Animals* (ed. S. Coombs, J. Janssen, J. F. Webb, J. Atema, R. R. Fay, A. N. Popper and W. Tavolga), pp. 151-186. New York: Springer.

Künzel, S., Bleckmann, H. and Mogdans, J. (2011). Responses of brainstem lateral line units to different stimulus source locations and vibration directions. *J. Comp. Physiol. A* **197**, 773-787.
McConney, M. E., Chen, N., Lu, D., Hu, H. A., Coombs, S., Liu, C. and Tsukruk, V. V. (2009). Biologically inspired design of hydrogel-capped hair sensors for enhanced underwater flow detection. *Soft Matter* **5**, 292-295.
Miyoshi, M. and Kaneda, Y. (1988). Inverse filtering of room acoustics. *IEEE Trans. Acoust. Speech Signal Process.* **36**, 145-152.
Mogdans, J. and Kröther, S. (2001). Brainstem lateral line responses to sinusoidal wave stimuli in the goldfish, *Carassius auratus*. *Zoology* **104**, 153-166.
Nelson, P. A., Hamada, H. and Elliott, S. J. (1992). Adaptive inverse filters for stereophonic sound reproduction. *IEEE Trans. Signal Process.* **40**, 1621-1632.
Oppenheim, A. V., Schafer, R. W. and Buck, J. R. (1989). *Discrete-Time Signal Processing*, 2nd edn. Upper Saddle River, NJ: Prentice Hall.